Experimental and Theoretical Study of Interlaminar Eddy Current Loss in Laminated Cores.

Sahas Bikram Shah*, Paavo Rasilo*,†, Anouar Belahcen*, and Antero Arkkio*
*Department of Electrical Engineering and Automation, Aalto University, P.O. Box 13000, FI-00076 Aalto, Finland
†Laboratory of Electrical Energy Engineering, Tampere University of Technology, Finland

***Abstract*—Insulation failure between the electrical sheets of electrical machines or transformers might occur due to the burrs formed during the cutting process. Together with welding seams or screws used to hold the stack together, the burrs provide a conducting path for eddy currents. In this paper, equivalent conductivities of the EI core with and without interlaminar contacts are determined using 3D finite element computations and measurements. The core loss of the EI core is measured, and the eddy current loss is segregated from the measurements. Based on the acquired eddy current loss, the equivalent conductivities are determined using an iterative approach. In the case of interlaminar fault at one limb, eddy current loss coefficient increased by 2% and in the case of interlaminar fault at two limbs, eddy current loss coefficient increased by 2.7% compared to the healthy case.**

***Index Terms*—burr, conductivity, eddy current loss, finite element method (FEM), interlaminar current, three dimensional (3D)**

I. Introduction

LAMINATION of the cores of electrical machines and transformers reduces the path of eddy current and hence reduces the eddy current loss. However, burrs are formed at the edges of electrical sheets during punching and deteriorate the insulation of adjacent sheets. The size of the burrs depends on the type of insulating material, insulating thickness, and age of the punching tool [1]. In electrical machines and transformers, the deterioration of the insulation also occurs due to excessive mechanical vibration and friction between laminations. Moreover, the stack of electrical steel sheets are held together by either welding or screws. Together with burrs, these provide a conducting path for eddy currents, which increases eddy current loss. In [2], the effect of welding on eddy current loss of a stack of electrical steel sheets was studied. The weld bead radius should be small to reduce the eddy current loss. It was also observed that the eddy current loss was higher in thinner electrical sheets and was more sensitive to welding than the thicker sheets. In [3], [4], the effect of interlaminar contacts in an induction machine was studied using finite element method, and it was observed that burrs particularly occur on the tooth edges and lead to a significant loss increase. In [5], [6], [7], an analytical approach was considered to calculate eddy current loss due to burrs at the edge of electrical sheets. It was observed that eddy current loss increased significantly as the number of shorted laminations increased. It is eminent to study these interlaminar contacts and their effect on the eddy current loss both experimentally and theoretically. In literature, there are many analytical and finite element approaches to study the interlaminar losses. However, the randomness of these interlaminar contacts is not addressed.

In a previous paper, we have proposed an efficient finite element method to account for interlaminar losses in electrical sheets due to random galvanic contacts [8]. The randomness of the galvanic contacts was modeled considering the conductivity as a random field and was solved using stochastic Galerkin finite element method. The quantification of the random conductivity and the equivalent conductivity of a stack of laminated sheets with interlaminar contacts still does not exist at present.

In this paper, we discuss the effect of interlaminar contacts on the eddy current loss of an EI core using measurement results and using $\mathbf{A} - V$ formulation in 3D finite element method. First, specific core losses of healthy and faulty EI cores are obtained from measurement, and specific eddy current losses are segregated for the healthy and faulty cores. Then, the equivalent conductivities of the healthy and faulty EI core are determined based on the obtained eddy current loss from measurement and using 3D finite element method. The effect of interlaminar contacts at two different positions of the EI core is also studied. In the case of the interlaminar fault at one limb, eddy current loss coefficient increased by 2% and in the event of the interlaminar fault at two limbs, eddy current loss coefficient increased by 2.7% compared to the healthy case.

II. Methods

The schematic of the EI core under study is shown in Figure 1. A controlled voltage waveform is supplied to the coil using power supply ELGAR SW 5250A. The controlled voltage ensures a sinusoidal induction in the EI core. This alternating flux causes eddy current loops in each sheet of the EI core. The modeling of each lamination of the core is computationally demanding hence homogenization of the core is needed. In [9], [10], equivalent conductivity of homogenized core was determined analytically based on the condition that the dissipated the power of a laminated core is equal to that of the homogenized core. In this paper, the core is modeled as a transversely isotropic solid conductor, with equal conductivities $\sigma_{\mathrm{x}} = \sigma_{\mathrm{b}}$ and $\sigma_{\mathrm{z}} = \sigma_{\mathrm{b}}$ in the x- and z-directions and a lower conductivity $\sigma_{\mathrm{y}} = \sigma_{\mathrm{h}}$ in the y- direction. An equivalent conductivity $\sigma_{\mathrm{y}} = \sigma_{\mathrm{h}}$ is defined as a value which gives the same specific eddy current loss as obtained

from the measurement. The determination of the equivalent conductivity allows us to calculate the eddy current loss of the EI core without discretizing each lamination.

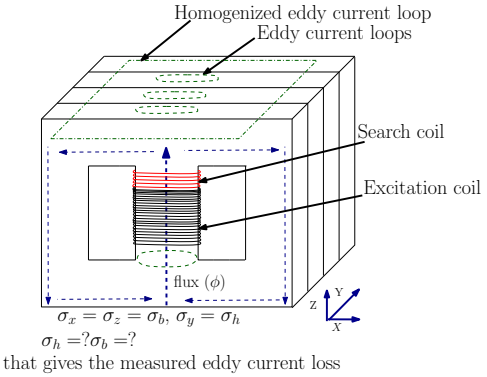

Fig. 1. Illustration of the EI core with lamination level eddy current loops and the homogenized behavior

1) Measurement:

a) Healthy core measurement: The EI core under study is shown in Figure 2. It consists of three limbs. An excitation winding is wound around the middle limb and the induced voltage is also measured at middle limb using the search coil. The no-load current is measured using Norma triax shunt LEM sensor. Dewetron-DWE-50-PCI-32 is used for data acquisition at the sampling rate of 100 kHz. The control algorithm developed in [11], [12] is used to ensure the sinusoidal excitation of the magnetic flux. The magnetic flux is obtained from the measured induced voltage at the central limb of the EI core. The no-load current and magnetic flux are obtained at different frequencies ranging from 5 Hz to 150 Hz. The specific core loss of the EI core is then calculated as (1).

$$p_{\text{Fe}} = \frac{1}{T}\frac{1}{m_{\text{Fe}}}\left[\int_0^T v(t)i(t)\text{d}t - i(t)^2 R_{\text{dc}}\right], \qquad (1)$$

where, R_{dc} and i are the measured dc resistance of the winding and supplied current, respectively. v is the supplied voltage that gives the sinusoidal excitation magnetic flux at the central limb. T is the time period and m_{Fe} is the mass of the EI core.

b) Faulty core measurement: Interlaminar short circuits between the sheets of the EI core are introduced by holding the conducting electrical sheet of the same material as that of the EI core at the opposite ends as shown in Figure 2. The sheets of the EI core are stacked as uniformly as possible to ensure that all the sheets are in contact. Two cases were studied. First interlaminar short circuits are applied to one of the limbs of the EI core, and secondly, interlaminar short circuits are applied to the left and right limbs of the EI core.

2) Loss segregation: The measured flux and current of the healthy and the faulty cores at frequencies 5 Hz and 150 Hz are shown in Figure 3 and Figure 4, respectively. At higher frequencies, the area enclosed by the flux and current loop is bigger due to eddy current. At 150 Hz, the eddy current loss is higher than the hysteresis loss. In the case of the faulty cores, the areas enclosed by the flux and current loops

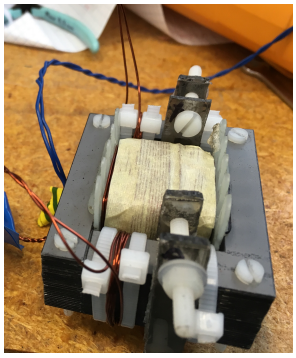

Fig. 2. Interlaminar fault at two limbs

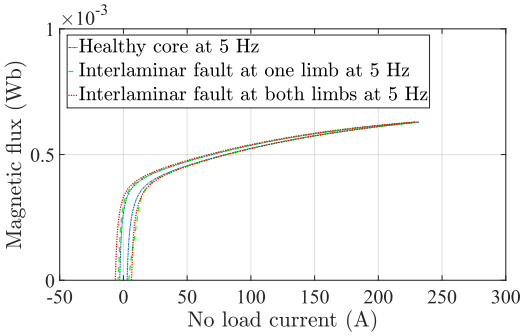

Fig. 3. Magnetic flux and no-load current loop at 1.5 T at 5 Hz

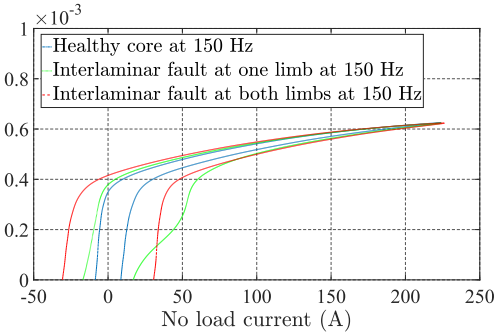

Fig. 4. Magnetic flux and no-load current loop at 1.5 T at 150 Hz

were bigger. When the interlaminar fault was applied to only one of the limbs, a distortion in magnetic flux was observed as shown in Figure 4. In the case of the interlaminar short circuits at one limb, the alternating main flux induces the interlaminar currents, and these interlaminar currents again induce the flux that reduces the main flux and increases the average eddy current loss at a given induction. In the case of a symmetrical interlaminar short circuit in both the right and left limbs, the interlaminar current induces the fluxes that reduce the main flux and increase the average eddy current loss. In the case of the interlaminar short circuit at one limb, higher harmonic flux is introduced and causes the distortion in the flux current loop as can be seen from Figure 4 and Figure 5. However, in the case of symmetrical interlaminar short circuits, higher harmonic fluxes cancel each other.

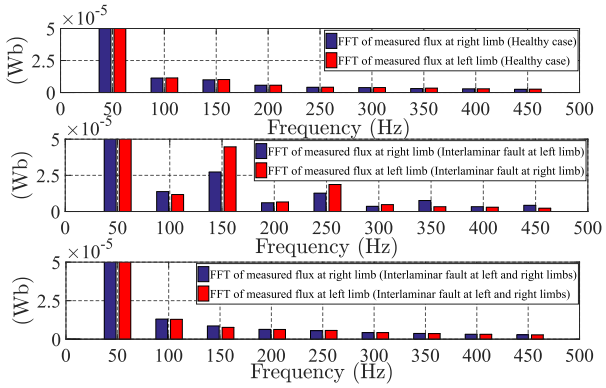

Fig. 5. An FFT of measured magnetic flux of healthy, one limb faulty and two limbs faulty EI core.

In both healthy and faulty cases, the specific losses were calculated using (1). The losses can be segregated from the specific core loss based on Steinmetz's early work [13], [14] and can be expressed as,

$$p_{\text{Fe}} = k_{\text{h}} f \hat{B}^n + k_{\text{e}} f^2 \hat{B}^2, \tag{2}$$

where, the first term of (2) represents the static hysteresis loss component and the second term represents the eddy current loss component. The coefficients are determined by dividing (2) by frequency and using least square curve fitting method [15].

$$\frac{p_{\text{Fe}}}{f} = \text{C} + \text{D}f \text{ where,} \tag{3}$$

$$\text{C} = k_{\text{h}} \hat{B}^n, \quad \text{D} = k_{\text{e}} \hat{B}^2. \tag{4}$$

The linear fitting of (3) gives the best goodness of fit of $R^2 \approx 0.99$. Hence, the coefficients of the polynomial in f can be calculated from the measured data for any induction of $\hat{B}$. $\hat{B}$ is the peak magnetic flux density. The polynomial coefficients C and D, are again fitted separately for different induction levels to determine the coefficients in (4). The static hysteresis loss is equivalent to C. The specific energy loss curves for the healthy and the faulty EI cores are shown in Figure 6. Finally,

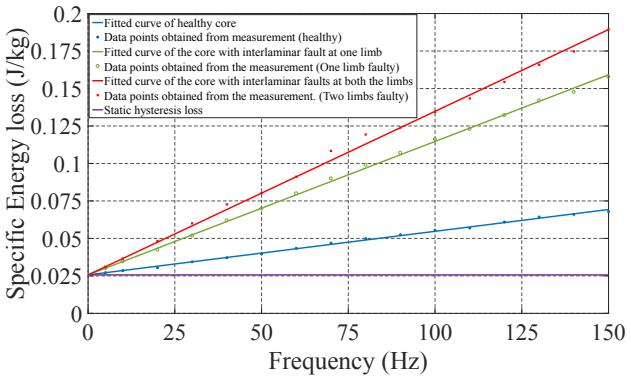

Fig. 6. Specific core loss per cycle at 1.5 T

the specific eddy current loss of the EI cores is calculated deducting the static hysteresis loss from the specific core loss. The specific eddy current loss of healthy and faulty EI cores are shown in Figure 7, respectively. The specific eddy current loss is calculated at an induction of 1.5 T to compare with the simulation results. The coefficients and the specific eddy

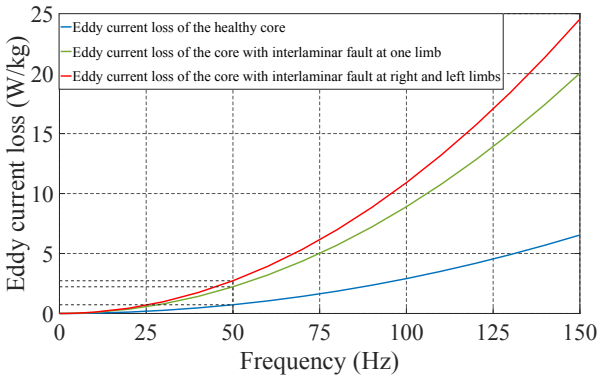

Fig. 7. Dynamic specific eddy current loss at 1.5 T

current loss for healthy and faulty cores are tabulated in Table I.

TABLE I
IRON-LOSS PARAMETERS OF HEALTHY AND FAULTY CORE AT 50 HZ 1.5 T

	Healthy core	**Core with one faulty limb**	**Core with two faulty limbs**
k_{h}, n [J/kgT$^{2.5}$]	0.0085, 2.5	0.0085, 2.5	0.0085, 2.50
k_{e} [J/kgHzT^2]	1.35 $\times 10^{-4}$	3.99 $\times 10^{-4}$	4.97 $\times 10^{-4}$
Eddy current loss [W/kg]	0.72	2.22	2.72

3) Simulation: Theoretical formulation:

a) Mathematical FEM formulation: The 3D eddy current formulation is based on **A**-V formulation. A finite element study of eddy current formulation is implemented in FEM software COMSOL. The quasi-magnetostatic Maxwell's equations are given by,

$$\mathbf{B} = \nabla \times \mathbf{A}, \tag{5}$$

$$\nabla \times \nu \nabla \times \mathbf{A} + \bar{\sigma}\mathbf{E} = \mathbf{J}_{\text{s}}, \tag{6}$$

where, ν, $\mathbf{A}$, $\bar{\sigma}$, $\mathbf{E}$ and $\mathbf{J}_{\text{s}}$ are the reluctivity, magnetic vector potential, conductivity tensor, electric field and external current density, respectively.

$$\mathbf{E} = -\nabla V - j\omega\mathbf{A} \tag{7}$$

The electric field is given by (7) and the external current density is calculated using the known supplied voltage, the resistance of the coil and its area. The angular frequency and the electric scalar potential is given by ω and V, respectively. The electric field is either produced from external sources or

induced surface charges. The continuity between two regions of different conductivity is ensured by imposing the normal component of current density to be continuous.

$$(-j\bar{\sigma}\omega\mathbf{A} - \bar{\sigma}\nabla V)\cdot\mathbf{n} = \mathbf{0} \tag{8}$$

The continuity of the tangential component of the electric field is ensured using edge elements in finite element discretization and the boundary condition (8) is imposed. The uniqueness of the solution of magnetic vector and electrical scalar potentials are ensured imposing the gauge condition and using iterative solver implemented in COMSOL [16], [17].

b) FEM implementation: The magnetic vector potential formulation is implemented in the EI core, and a frequency domain analysis of Maxwell's equations is solved. The primary voltage that induces sinusoidal flux excitation in the core of amplitude 1.5 T is considered in simulation. An FFT is done to the measured primary voltage to obtain the magnitude and phase angle of the supplied voltage. It is then used as the source term in finite element computation. The nonlinearity of the material in the simulation is considered using the effective magnetization curve which originates from the nonlinear BH curve of the material [18].

$$\nu_{\text{eff}} = \frac{1}{T}\int_T \frac{H(t)}{\hat{B}\sin(2\pi t/T))}\mathrm{d}t \tag{9}$$

There are many methods to create effective magnetization curve in literature [19], [20], but in this paper, the effective permeability is calculated as equation (9), which considers sinusoidal magnetic flux density and considers the fundamental frequency only [21], [22]. ν_{eff} is the effectve reluctivity, H is the magnetic field, T is the time period and $\hat{B}$ is the peak magnetic flux density, respectively.

4) Proposed method: The finite element study of the EI core is done with finely discretized tetrahedral and edge elements. The conductivities in x and y-direction are varied from 1 S/m to 2.7×10^6 S/m, and frequency domain finite element simulation is performed.

$$p_{\text{ed}} = \frac{\int_{\text{V}} \frac{1}{2}\mathbf{E}\cdot\mathbf{J}^*_{\text{ind}}\mathrm{dV}}{m_{\text{Fe}}}. \tag{10}$$

The eddy current loss is calculated using (10) for each finite element simulation that corresponds to all possible sets of conductivities. $\mathbf{J}_{\text{ind}}$ is the induced current density and V is the volume of the EI core. The eddy current losses calculated for the healthy and faulty EI cores are shown in Figure 8. A response surface of the eddy current loss is then obtained for all possible sets of conductivities of σ_{h} and σ_{b}. It is obtained for both the healthy and faulty cases using the bicubic spline fitting tool in Matlab. The response surfaces of the healthy, one limb fault and two limbs fault EI core are shown in Figure 9, Figure 10 and Figure 11, respectively. First, the equivalent conductivities of the healthy EI core are obtained iteratively based on the measured eddy current loss using the response surface of the healthy core. The algorithm of the iterative process is shown in Figure 12. The conductivity of the electrical sheet in x- and z- directions is σ_{b} and in the

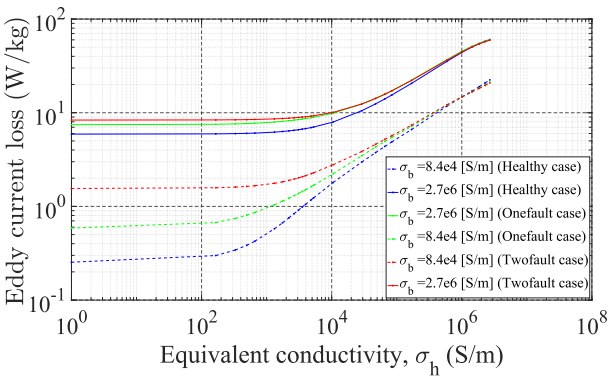

Fig. 8. Eddy current loss at different conductivities

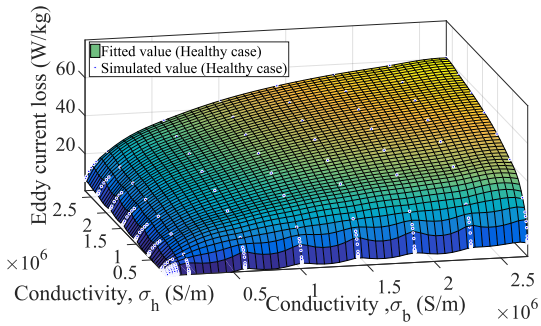

Fig. 9. Response surface of the eddy current loss for healthy case

perpendicular direction to the laminated sheets is σ_{h} as shown in Figure 1. The conductivity σ_{b} is initialized with 2.7×10^6 S/m, which is the conductivity of the electrical steel. The specific eddy current loss as a function of σ_{h} is obtained at each σ_{b} from the corresponding response surface. Then, Newton's method is used to obtain the equivalent conductivity σ_{h} that gives the measured specific eddy current loss. It is assumed that interlaminar contacts only effect the conductivity in y direction i.e. along the laminated direction. Hence, fixing the σ_{b} obtained from the healthy core, σ_{h} is obtained iteratively for the faulty cases using the obtained response surfaces.

III. Results and Discussion

In the case of the healthy EI core in which there are no interlaminar circulating currents, the eddy current loss was obtained from measurement as 0.72 W/kg. The other source of interlaminar current was reduced by using plastic nuts and bolts to hold the EI sheets together. The iterative solution of the conductivities for the measured loss is tabulated in Table II. The equivalent conductivity (σ_{h}) of the EI core with one limb fault and two limbs fault increased to 1.057×10^4 S/m and 1.4668×10^4 S/m, respectively. However, these conductivities depend on interlaminar fault area. The higher the fault area, the higher will be the conductivity. The solution of the magnetic flux density and the current density at those conductivities for the healthy case are shown in Figure 13 and Figure 14, respectively. Similarly, the solution of magnetic flux density and

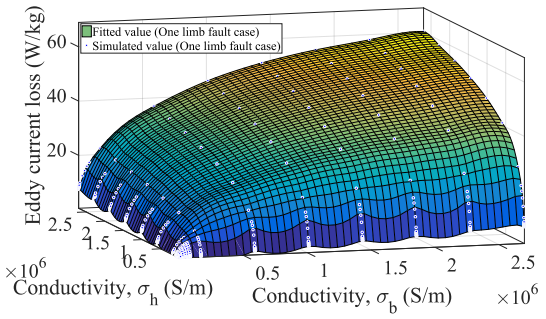

Fig. 10. Response surface of the eddy current loss for the onefault limb case

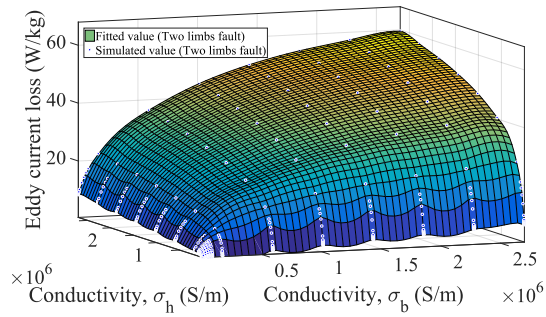

Fig. 11. Response surface of the eddy current loss for twofault case

TABLE II
EQUIVALENT CONDUCTIVITY OF HEALTHY AND FAULTY CORE

	Healthy core	**Core with one faulty limb**	**Core with two faulty limbs**
σ_b	5×10^5 S/m	5×10^5 S/m	5×10^5 S/m
σ_h	4 S/m	1.057×10^4 S/m	1.4668×10^4 S/m

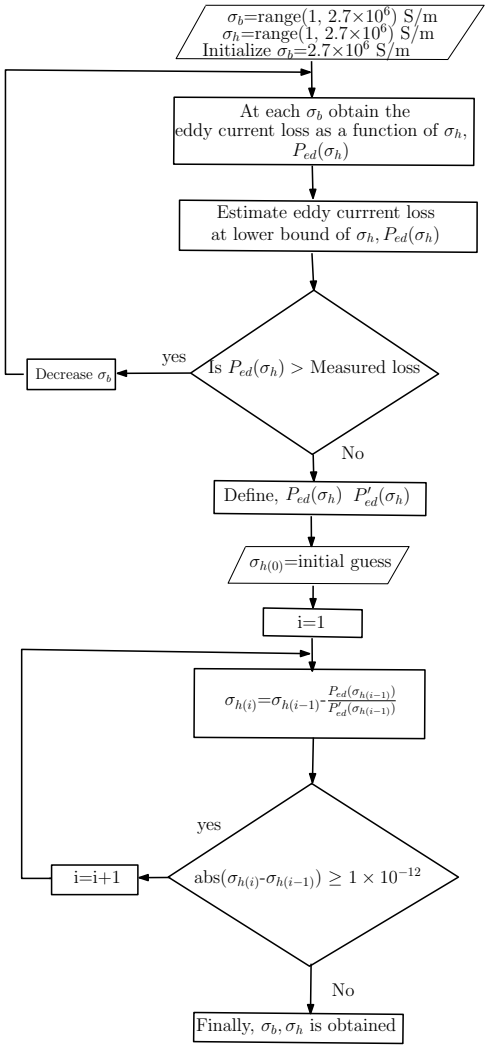

Fig. 12. Flowchart of iterative process

current density for faulty cases are shown in Figure 15, Figure 16, Figure 17 and Figure 18. In the case of the interlaminar contacts, the induced current density is increased significantly, and in the case of higher frequency the induced current is large enough to create a hotspot and destroy the insulation and core. However, the effect of interlaminar contacts also depend on the surface coating of the electrical sheets. These interlaminar contacts are stochastic in nature and mainly depend on the age of the punching tool, stamping pressure and coatings properties.

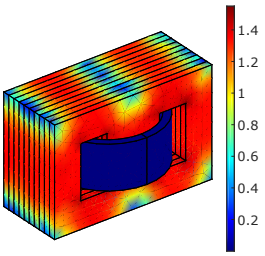

Fig. 13. Magnetic flux density (T) at 50 Hz (Healthy case)

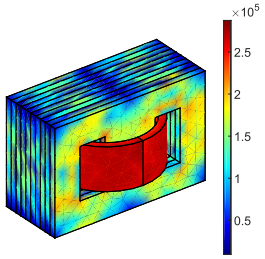

Fig. 14. Induced current density (A/m^2) at 50 Hz (Healthy case)

IV. CONCLUSION

The effect of interlaminar contacts on the equivalent conductivities of the EI core was studied. In the case of the interlaminar fault at one limb, eddy current loss coefficient increased by 2% and in the case of the interlaminar fault at two limbs, eddy current loss coefficient increased by 2.7% compared to the healthy case. The study is based on the measurement and three-dimensional finite element simulations. The deduced specific eddy current loss from the measurement is used to obtain the equivalent conductivities using an iterative approach and finite element method. These equivalent conductivities can be used to model the laminated sheets in three-dimensional finite element method using $\mathbf{A}$-V formulation. Moreover, this study also determines the increased equivalent conductivity of the laminated sheets due to interlaminar contacts. The obtained equivalent conductivities can be used in sensitivity analysis during the design of transformers and

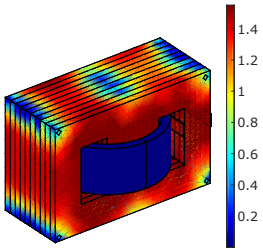

Fig. 15. Magnetic flux density (T) at 50 Hz (One limb fault case)

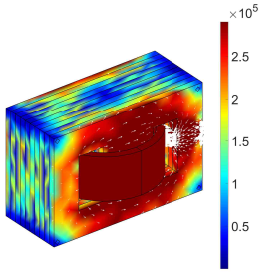

Fig. 16. Induced current density (A/m^2) at 50 Hz (One limb fault case)

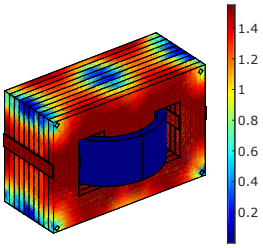

Fig. 17. Magnetic flux density (T) at 50 Hz (Two limbs fault case)

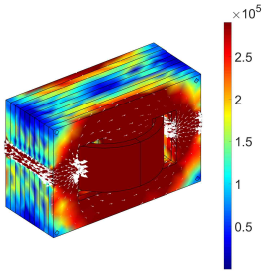

Fig. 18. Induced current density (A/m^2) at 50 Hz (Two limbs fault case)

electrical machines. It can also provide an estimate of the upper and the lower bounds of conductivities in the stochastic study of the eddy current loss considering random interlaminar contacts.

ACKNOWLEDGMENT

The research leading to these results has received funding from the European Research Council under the European Unions Seventh Framework Programme (FP7/2007-2013) ERC grant agreement no 339380. This work was also supported in part by the Academy Finland under grant 274593. The author would like to thank Dr. Deepak Singh and Dr. Floran Martin for their useful suggestions during measurement.

REFERENCES

[1] A. C. Beiler and P. L. Schmidt, "Interlaminar eddy current loss in laminated cores," *Transactions of the American Institute of Electrical Engineers*, vol. 66, no. 1, pp. 872–878, Jan 1947.

[2] H. Wang and Y. Zhang, "Modeling of eddy-current losses of welded laminated electrical steels," *IEEE Transactions on Industrial Electronics*, vol. 64, no. 4, pp. 2992–3000, April 2017.

[3] P. Handgruber, A. Stermecki, O. Br, and G. Ofnery, "Evaluation of interlaminar eddy currents in induction machines," in *Industrial Electronics Society, IECON 2013 - 39th Annual Conference of the IEEE*, Nov 2013, pp. 2792–2797.

[4] S. B. Shah, P. Rasilo, A. Belahcen, and A. Arkkio, "Estimation of additional losses due to random contacts at the edges of stator of an electrical machine," *COMPEL - The international journal for computation and mathematics in electrical and electronic engineering*, vol. 34, no. 5, pp. 1501–1510, 2015. [Online]. Available: http://dx.doi.org/10.1108/COMPEL-02-2015-0083

[5] H. Hamzehbahmani, P. Anderson, J. Hall, and D. Fox, "Eddy current loss estimation of edge burr-affected magnetic laminations based on equivalent electrical network part i: Fundamental concepts and fem modeling," *IEEE Transactions on Power Delivery*, vol. 29, no. 2, pp. 642–650, April 2014.

[6] H. Hamzehbahmani, P. Anderson, and A. Eldieb, "An overview of the recent developments of the inter-laminar short circuit fault detection methods in magnetic cores," in *Power Engineering Conference (UPEC), 2015 50th International Universities*, Sept 2015, pp. 1–7.

[7] Ziani, Smail, Henneron, Thomas, Puigdellivol, Oriol, and Le Menach, Yvonnick, "A method coupling modified vector potential a* and homogenization formulations to model short-circuits in lamination stacks," *Eur. Phys. J. Appl. Phys.*, vol. 75, no. 3, p. 30901, 2016. [Online]. Available: https://doi.org/10.1051/epjap/2016160026

[8] S. B. Shah, P. Rasilo, H. Hakula, and A. Arkkio, "Efficient finite element method to estimate eddy current loss due to random interlaminar contacts in electrical sheets," *International Journal of Numerical Modelling: Electronic Networks, Devices and Fields*, 2017.

[9] P. Hahne, R. Dietz, B. Rieth, and T. Weiland, "Determination of anisotropic equivalent conductivity of laminated cores for numerical computation," *IEEE Transactions on Magnetics*, vol. 32, no. 3, pp. 1184–1187, May 1996.

[10] A. Bermudez, D. Gomez, and P. Salgado, "Eddy-current losses in laminated cores and the computation of an equivalent conductivity," *IEEE Transactions on Magnetics*, vol. 44, no. 12, pp. 4730–4738, Dec 2008.

[11] D. Singh, "Effect of stress on magnetic properties of electrical steel sheet and core losses in electrical machines," pp. 108 + app. 54, 2016. [Online]. Available: http://urn.fi/URN:ISBN:978-952-60-7233-3

[12] P. Rasilo, D. Singh, U. Aydin, F. Martin, R. Kouhia, A. Belahcen, and A. Arkkio, "Modeling of hysteresis losses in ferromagnetic laminations under mechanical stress," *IEEE Transactions on Magnetics*, vol. 52, no. 3, pp. 1–4, March 2016.

[13] C. P. Steinmetz, "On the law of hysteresis," *Transactions of the American Institute of Electrical Engineers*, vol. IX, no. 1, pp. 1–64, Jan 1892.

[14] ——, "On the law of hysteresis (part ii.) and other phenomena of the magnetic circuit," *Transactions of the American Institute of Electrical Engineers*, vol. IX, no. 1, pp. 619–758, Jan 1892.

[15] D. M. Ionel, M. Popescu, S. J. Dellinger, T. J. E. Miller, R. J. Heideman, and M. I. McGilp, "On the variation with flux and frequency of the core loss coefficients in electrical machines," *IEEE Transactions on Industry Applications*, vol. 42, no. 3, pp. 658–667, May 2006.

[16] *AC/DC Module User's Guide, pp. 243-247*, COMSOL Multiphysics v.5.2, COMSOL AB, Stockholm, Sweden, 2015.

[17] Z. Ren, "Influence of the rhs on the convergence behaviour of the curl-curl equation," *IEEE Transactions on Magnetics*, vol. 32, no. 3, pp. 655–658, May 1996.

[18] G. Paoli, O. Biro, and G. Buchgraber, "Complex representation in nonlinear time harmonic eddy current problems," *IEEE Transactions on Magnetics*, vol. 34, no. 5, pp. 2625–2628, Sep 1998.

[19] O. Biro, K. Preis, and K. R. Richter, "Various fem formulations for the calculation of transient 3d eddy currents in nonlinear media," *IEEE Transactions on Magnetics*, vol. 31, no. 3, pp. 1307–1312, May 1995.

[20] G. Paoli and O. Br, "Time harmonic eddy currents in nonlinear media," *COMPEL - The international journal for computation and mathematics in electrical and electronic engineering*, vol. 17, no. 5, pp. 567–575, 1998. [Online]. Available: http://dx.doi.org/10.1108/03321649810220865

[21] J. Pippuri and A. Arkkio, "Time-harmonic induction-machine model including hysteresis and eddy currents in steel laminations," *IEEE Transactions on Magnetics*, vol. 45, no. 7, pp. 2981–2989, July 2009.

[22] A. Niemenmaa, "Complex reluctivity modelling of iron losses in induction machines," in *Proceedings of Internation Conference on Electrical Machines*, vol. 1, Pisa, Italy, 1988, pp. 633–636.